© 2021. Published by The Company of Biologists Ltd | Development (2021) 148, dev199687. doi:10.1242/dev.199687

RESEARCH ARTICLE

TECHNIQUES AND RESOURCES

Visualizing the organization and differentiation of the male-specific nervous system of *C. elegans*

Tessa Tekieli[1], Eviatar Yemini[1], Amin Nejatbakhsh[2], Chen Wang[1], Erdem Varol[2], Robert W. Fernandez[1], Neda Masoudi[1], Liam Paninski[2] and Oliver Hobert[1,*]

ABSTRACT

Sex differences in the brain are prevalent throughout the animal kingdom and particularly well appreciated in the nematode *Caenorhabditis elegans*, where male animals contain a little-studied set of 93 male-specific neurons. To make these neurons amenable for future study, we describe here how a multicolor reporter transgene, NeuroPAL, is capable of visualizing the distinct identities of all male-specific neurons. We used NeuroPAL to visualize and characterize a number of features of the male-specific nervous system. We provide several proofs of concept for using NeuroPAL to identify the sites of expression of *gfp*-tagged reporter genes and for cellular fate analysis by analyzing the effect of removal of several developmental patterning genes on neuronal identity acquisition. We use NeuroPAL and its intrinsic cohort of more than 40 distinct differentiation markers to show that, even though male-specific neurons are generated throughout all four larval stages, they execute their terminal differentiation program in a coordinated manner in the fourth larval stage. This coordinated wave of differentiation, which we call 'just-in-time' differentiation, couples neuronal maturation programs with the appearance of sexual organs.

KEY WORDS: *C. elegans*, Nervous system, Sex specific

INTRODUCTION

It is generally appreciated that nervous systems are sexually dimorphic on a gross anatomical level. However, sex differences in nervous systems have been carefully mapped out, with single-cell resolution, in only very few animals. The nematode *Caenorhabditis elegans* is the only organism for which a complete cellular, lineage and anatomical map of the entire nervous system has been described for both sexes (Fig. 1) (Cook et al., 2019; Jarrell et al., 2012; Sulston et al., 1980; Sulston and Horvitz, 1977). With 387 neurons in total, the nervous system of the male is almost 30% larger than that of the hermaphrodite (302 neurons). Based on position, lineage, anatomy and molecular features, 294 neurons are shared between both sexes. Hermaphrodites, which are somatic females, contain an additional eight hermaphrodite-specific neurons that fall into two classes: the well-characterized HSN and VC motor neuron classes, both of which control egg laying behavior (Schafer, 2005). The male contains an additional 93 neurons that fall into 27 anatomically distinct classes (Fig. 1, Table S1) (Cook et al., 2019; Molina-Garcia et al., 2020; Sammut et al., 2015; Sulston et al., 1980), two located in the head (sensory neuron classes CEM and MCM), two in the ventral nerve cord (motor neuron classes CA and CP), and the remaining, heavily interconnected 23 classes located in the tail of the animal. With the exception of the four CEM sensory neurons in the head, which are born in the embryo and induced to die in hermaphrodites, all male-specific neurons are generated during postembryonic development from blast cells that proliferate, survive and differentiate in a male-specific manner (Fig. 1B) (Molina-Garcia et al., 2020; Sammut et al., 2015; Sulston et al., 1980). Based on cell division patterns, the 89 postembryonically generated male-specific neurons are generated at different larval stages. Each individual larval stage contributes to the generation of some of these postembryonic neurons (Sulston et al., 1980). However, when exactly these neurons terminally differentiate is poorly understood. Moreover, in his classic lineage studies Sulston et al. also noted that the number of two male-specific neuron classes, DX and EF, display a variable number of class members (Sulston et al., 1980). Similar variabilities in cell cleavage patterns have not been observed elsewhere within or outside the nervous system of *C. elegans*.

Despite many interesting aspects of the male nervous system, it has received little attention over the years compared with the nervous system of the hermaphrodite. A number of studies have illuminated aspects of the development and function of male-specific neurons, but those studies only dealt with a limited set of neurons (Barr et al., 2018; Emmons, 2014, 2018; Garcia et al., 2001; Garcia and Portman, 2016; Liu and Sternberg, 1995; Portman, 2017). Hence, many aspects of the development and function of the 93 male-specific neurons remain uncharted territory. With some notable exceptions, including the systematic mapping of neurotransmitter identities (Gendrel et al., 2016; Pereira et al., 2015; Serrano-Saiz et al., 2017), and marker analysis in the ray sensory neurons (Lints et al., 2004) and ventral nerve cord (Kalis et al., 2014), few molecular markers have been developed that label male-specific neurons. Single-cell transcriptome approaches have so far exclusively focused on the hermaphrodite (Cao et al., 2017; Packer et al., 2019; Taylor et al., 2021). This dearth of molecular markers complicates the means by which cellular expression patterns in the male tail can be unambiguously identified and therefore limits the ability to assess cell fate in specific mutant backgrounds.

Here, we address these shortcomings by showing that NeuroPAL, a previously described multicolor transgene that distinguishes all neuron classes in hermaphrodites (Yemini et al., 2021), can also be used to disambiguate the 93 neurons of the male nervous system. We find that the NeuroPAL transgene, which harbors more than 40 promoters that drive the expression of four distinct fluorophores, generates a color map that provides sufficient discriminatory power

[1]Department of Biological Sciences, Howard Hughes Medical Institute, Columbia University, New York, NY 10027, USA. [2]Departments of Statistics and Neuroscience, Grossman Center for the Statistics of Mind, Center for Theoretical Neuroscience, Zuckerman Institute, Columbia University, New York, NY 10027, USA.

*Author for correspondence (or38@columbia.edu)

E.Y., 0000-0003-1977-0761; A.N., 0000-0001-5155-4757; O.H., 0000-0002-7634-2854

Received 7 April 2021; Accepted 16 August 2021

Development (2021) 148, dev199687. doi:10.1242/dev.199687

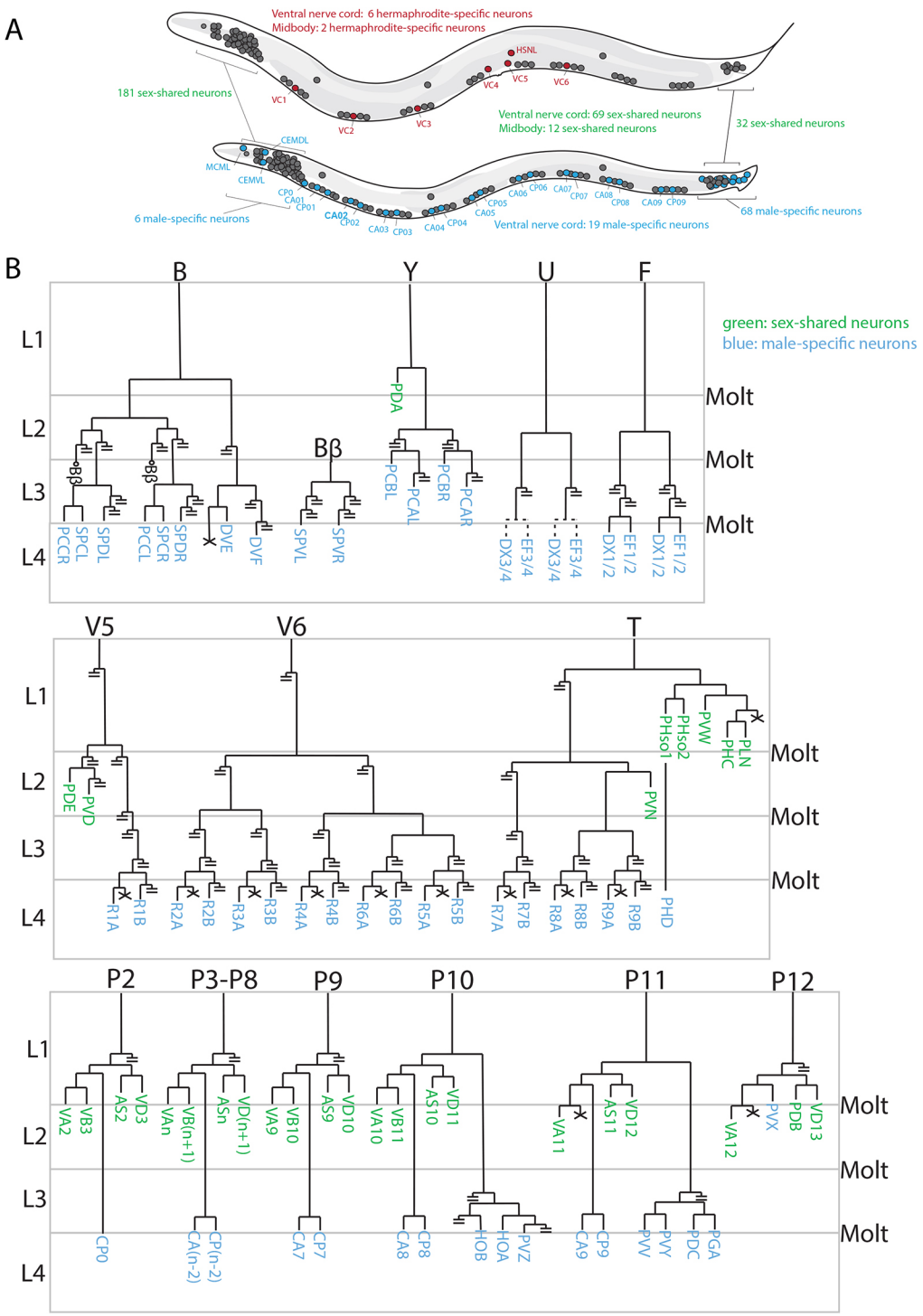

Fig. 1. Male-specific neurons and the timing of their generation. (A) Schematic overview of sex-specific neurons of the hermaphrodite (top) or male (bottom) *C. elegans* nervous systems. (B) Abridged version of the Sulston et al. (1980) lineage diagram of male-specific neurons in the tail. Only those branches that generate neurons are shown to the end, cells that die are denoted with an X, and all other branches are cut off (with double strike through). Note that male-specific neurons are generated at different times of larval development, with the earliest being generated at the L1 stage (PVX) and the latest being generated at the early L4 stage (DX, EF and rays). The lineage of the embryonically generated male-specific CEM neurons is not shown.

to identify all male-specific neurons reliably. We provide proof-of-principle examples that show how to use NeuroPAL to identify gene expression patterns in the nervous system, and we use the NeuroPAL color map to provide a number of insights into the development of the male-specific nervous system.

RESULTS

NeuroPAL provides discriminatory color barcodes for all male-specific neurons

With the exception of neurotransmitter pathway genes (Gendrel et al., 2016; Lints and Emmons, 1999; Pereira et al., 2015; Serrano-Saiz et al., 2017), few molecular markers have been comprehensively described throughout the entire male-specific nervous system (www.wormbase.org). For several related neuron classes, for example the ray neurons, molecular markers are available, but they do not provide sufficient resolution to distinguish between all individual class members (Lints and Emmons, 1999; Lints et al., 2004). We set out to test whether the NeuroPAL transgene that we previously described for the *C. elegans* hermaphrodite (Yemini et al., 2021) would provide a similarly information-rich molecular map of the male-specific nervous system.

Development (2021) 148, dev199687. doi:10.1242/dev.199687

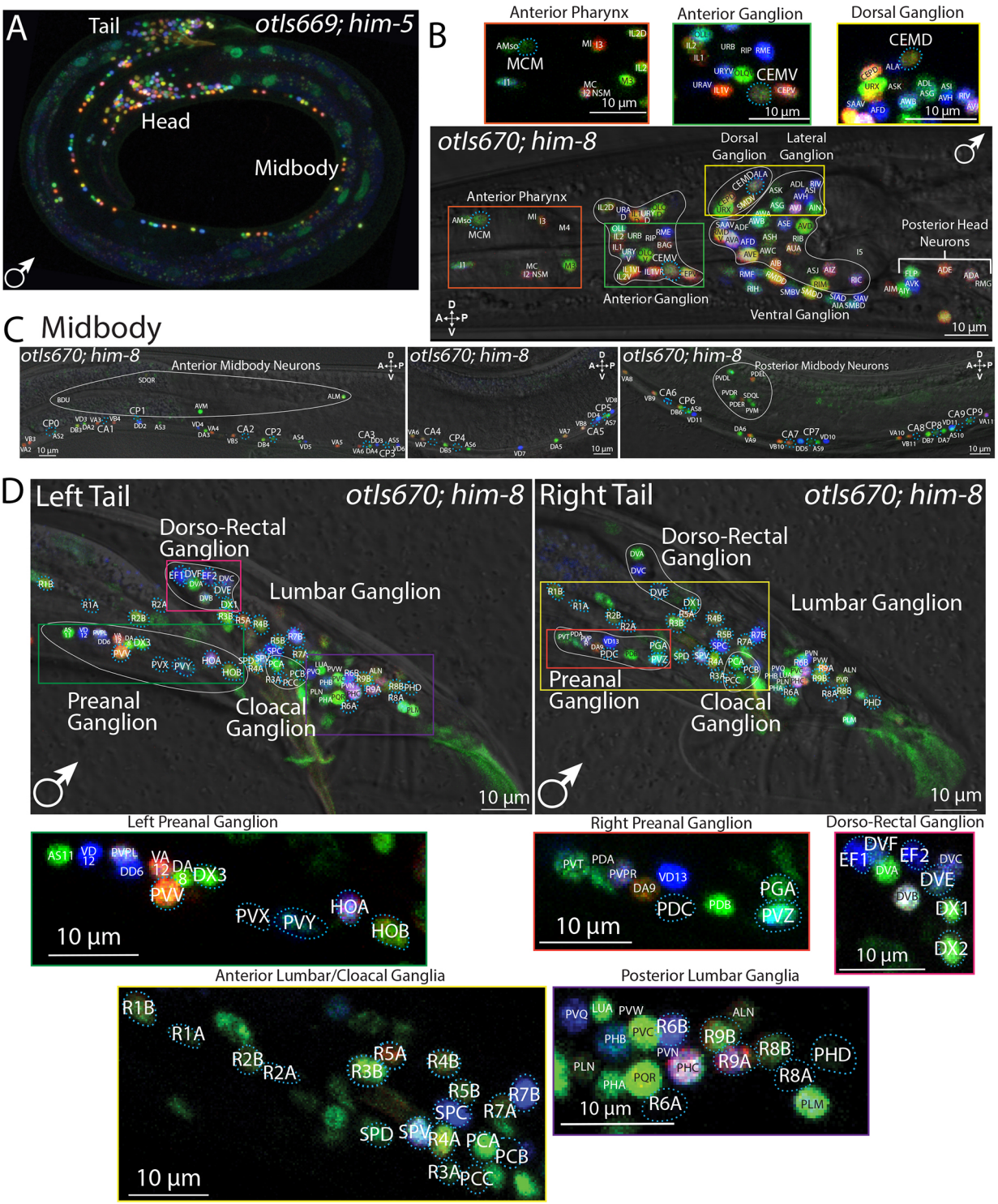

Fig. 2. Multicolor map of the adult, male-specific nervous system. (A) Overview of entire male NeuroPAL worm (*otIs669;him-5*) with the head, midbody and tail regions indicated. (B) Micrograph of a stereotypic adult male NeuroPAL (*otIs670; him-8*) head with inset images of regions in the male head containing male-specific neurons. These inset images correspond to the anterior pharynx (outlined in orange), the anterior ganglion (outlined in green), and the dorsal ganglion (outlined in yellow). All male-specific neurons are indicated with blue dashed circles. (C) Micrographs of stereotypic images from the midbody and ventral nerve cord of adult male NeuroPAL (*otIs670; him-8*) worms from anterior to posterior. All male-specific neurons are indicated with blue dashed circles. A, anterior; D, dorsal; P, posterior; V, ventral. (D) Stereotypic micrographs of the left and right side of male NeuroPAL tails with magnified images of indicated regions below. These magnified images correspond to the left preanal ganglion (outlined in green), the right preanal ganglion (outlined in orange), the dorso-rectal ganglion (outlined in magenta), the anterior lumbar/cloacal ganglia (outlined in yellow) and the posterior lumbar ganglia (outlined in purple). All male-specific neurons are indicated with blue dashed circles. In response to our lasers, the male spicules exhibit yellow autofluorescence and the tip of the male fan exhibits green autofluorescence.

Development (2021) 148, dev199687. doi:10.1242/dev.199687

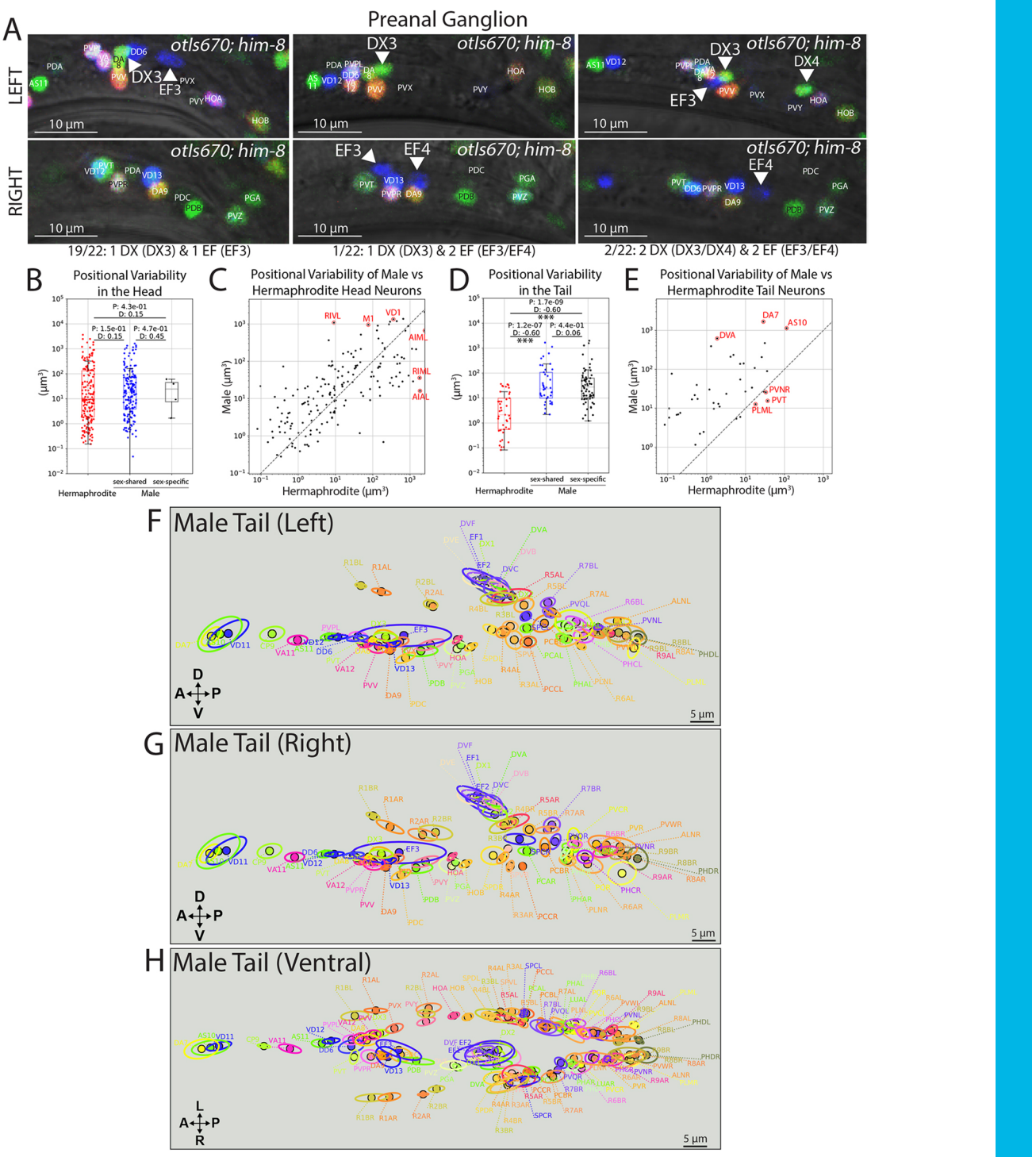

Fig. 3. Variability of cell generation and positions in the adult male tail. (A) NeuroPAL (*otIs670; him-8*) is used to visualize the variability of DX and EF neuron (DX3 and 4, and EF3 and 4) generation in the preanal ganglion of the adult male tail. Example images of the left and right sides (top and bottom, respectively) of the male preanal ganglion are shown in NeuroPAL worms. These images depict real observations of the indicated number of DX and EF neurons. The fraction of NeuroPAL worms observed, with the indicated DX/EF neuron count, is listed below the set of images exemplifying the indicated numbers of DX and EF neurons. Arrowheads indicate the EF and DX neurons in the images. (B-E) Quantification of positional variability for the collection of all head (B,C) and tail (D,E) neurons of the hermaphrodite (which are all sex-shared) versus the male sex-shared and sex-specific neurons. In the head, the positional variability is nearly the same (B,C). In the tail (D,E), the positional variability for the group of hermaphrodite neurons is far less than that of the male sex-shared and sex-specific neurons. Six neurons that show maximal differences between both sexes are circled and identified (C,E). Shown are the *P*-values (Mann–Whitney U test) for differences between hermaphrodites and males and the effect size (Cohen's D). For the head, *n*=10 hermaphrodites, 12 males, 182 sex-shared neurons, and 6 male-specific neurons, with a mean of 9.6 neurons/hermaphrodite and 9.8 neurons/male. For the tail, *n*=10 hermaphrodites, 13 males, 41 sex-shared neurons, and 69 male-specific neurons, with a mean of 9.6 neurons/hermaphrodite and 11.6 neurons/male. (F-H) The atlas of male tail neuron positional variability (based on 13 male tails) for the left (F), right (G) and ventral (H) sided views. Dots indicate the mean position of each neuron. Ellipses indicate the positional variability of each neuron in the given axis. Neuron colors are caricatured to approximate those in NeuroPAL but have been brightened for visibility. Further hermaphrodite and male atlases can be found in Fig. S2. Data are available in Table S2.

Development (2021) 148, dev199687. doi:10.1242/dev.199687

The NeuroPAL transgene was designed to provide color codes to all neurons of the *C. elegans* hermaphrodite (Yemini et al., 2021). This was achieved through the judicious use of four fluorophores with separable emission spectra (mTagBFP2, CyOFP1, Tag-RFP-T, mNeptune2.5), expressed under the control of a set of 43 different promoters with overlapping expression profiles [39 neuron type-specific promoters plus a synthetic ultra-pan-neuronal (UPN) driver made up of the *cis*-regulatory elements of four distinct, but fused, pan-neuronal promoters] (Yemini et al., 2021). Promoter choices were dictated by the goal of having neighboring neurons display distinct color codes, thereby unambiguously discriminating between neighboring neuron identities.

We found that three NeuroPAL transgenes (independently integrated transgenes *otIs696*, *otIs669* and *otIs670*) distinguish all neighboring male-specific neurons from one another. This is illustrated in the whole-animal overview in Fig. 2A along with large-scale images of all regions of the *C. elegans* nervous system that contain male-specific neurons (Fig. 2B-D, Fig. S1). The origin of the color code for each neuron is listed in Table S1. For several of the neuron classes, we do not know from which driver the fluorophore color derives, but this is not relevant for providing disambiguation between neighboring neurons. NeuroPAL not only provides color codes for neuron classes for which few or no molecular markers were previously available, but it also distinguishes neuronal subclasses that could previously not be discriminated. For example, individual subclasses of A- and B-type ray neurons subtypes can all be distinguished based on color code and position (Fig. 2, Table S1).

Using NeuroPAL to address stereotypy in the male-specific nervous system

We first used NeuroPAL to address questions that relate to stereotypy of the male-specific nervous system. In the original lineage analysis of the male tail, an unusual phenomenon, not observed anywhere else in the entire organism was reported: descendants of the U ectoblast produce variable numbers of DX and EF neurons, a notion indicated by stippled lines in the original lineage diagram (Sulston et al., 1980) (redrawn here in Fig. 1B). This contrasts the complete stereotypy and deterministic nature of all other *C. elegans* cell lineages, both neuronal and non-neuronal (Sulston et al., 1980; Sulston and Horvitz, 1977). Moreover, this variability was reported to be restricted to the EF and DX neurons that descend from the U neuroblast and that are located in the preanal ganglion (the EF3 and 4, and DX3 and 4 neurons). In contrast, the DX and EF neurons that are produced from the F neuroblast (EF1 and 2, DX1 and 2), located in the dorsal rectal ganglion, were generated in an apparently invariant manner (Sulston et al., 1980) (Fig. 1B). However, no quantification of this observation was provided. Also, because the lineage analysis relied on cleavage pattern alone, the extent to which the variably produced DX and EF neurons acquire a differentiated state was also not clear.

Using the distinctive NeuroPAL color codes for DX and EF neurons, we examined 22 young adult males and found variability in the presence of fully differentiated EF and DX neurons in the preanal ganglion, as assessed by wild-type expression of NeuroPAL colors in these neurons (Fig. 3A). Within the F-derived dorsorectal ganglion, 22/22 animals invariably showed two fully differentiated DX (DX1 and DX2) and two fully differentiated EF neurons (EF1 and EF2), corroborating the classic lineage report (Sulston et al., 1980). In the U-derived preanal ganglion, 19/22 animals showed one DX and one EF neuron (DX3 and EF3), 1/22 had one additional EF (EF4), and 2/22 had one additional EF (EF4) and one additional DX (DX4) neuron.

The EF and DX neurons are also the neurons with the greatest inter-animal variability in their relative positioning, as inferred by closely considering the overall variability of positioning of both sex-shared and sex-specific neurons in the tail of the animal. We had previously measured positional variability for neurons in the hermaphrodite head, where the vast majority of neurons are generated embryonically (Yemini et al., 2021); here, we observed a similar extent of variability in the male head, despite the addition of six male-specific neurons (Fig. 3B,C, Fig. S2A-C, Table S2). However, in the tail, where the vast majority of the postembryonically added male-specific neurons are located, there was substantially more positional variability, both in the sex-shared neurons as well as in the sex-specific neurons (Fig. 3D-H, Table S2). The EF and DX neurons stand out in the extent of variability in their positioning. It will be interesting to investigate whether the inter-animal variability in neuronal soma position in the male tail also translates into variability in neuronal process adjacency, and hence connectivity, between individual animals.

Using NeuroPAL to characterize reporter gene expression patterns in the male tail

Compared with the hermaphrodite nervous system, there is a remarkable scarcity of molecular markers for neurons in the male tail. The vast majority of reporter transgenes that researchers generate to analyze the expression of their gene of interest are usually only examined in hermaphrodites. One reason for the reluctance of identifying sites of reporter gene expression in the male tail has been the absence of reliable landmark reporters for most male-specific neurons. The fluorescence emission properties of NeuroPAL are designed to be separable from those of GFP signals. This allows researchers to overlay a GFP signal from a reporter gene of interest onto the neuron-specific color barcodes of NeuroPAL, thus identifying the sites of expression of GFP (or CFP/YFP)-based reporter transgenes. As a proof of principle, we analyzed CRISPR/Cas9-engineered *gfp*-based reporter alleles of three neuropeptide-encoding genes that were previously uncharacterized in males (*flp-3*, *flp-27* and *nlp-51*). To do so, we crossed these *gfp*-tagged alleles into a NeuroPAL background. We found that *flp-3::T2A::3xNLS::gfp* was expressed in the male-specific CA1, CA2, CA3 and CA4 neurons, located in the ventral nerve cord, as well as the male-specific R4A and SPV neurons in the tail (Fig. 4A**)**. We found that *flp-27::T2A::3xNLS::gfp* was expressed in the male-specific neurons CEMV, CEMD, CA8, CA9, PGA and R7A, and was dimly and variably expressed in R6B as well as the sex-shared neuron ASG **(**Fig. 4B). *nlp-51::SL2::GFP::H2B* was expressed in the male-specific PVX, R3B and PHD neurons in the tail and variably in R4B (Fig. 4C); in addition, non-dimorphic expression was observed in the sex-shared neurons AIM, RIP and PVN (Fig. 4C). These expression patterns corroborate the molecular diversity of members of the CA-type ventral nerve cord motor neurons, and that of the ray sensory neurons, as noted previously with other markers (Kalis et al., 2014; Lints et al., 2004).

Using NeuroPAL to measure neuronal cell-fate specification in the male tail

As described above, NeuroPAL is an indicator of expression for 39 neuron-type specific genes, as well as four pan-neuronal genes (the enhancers of which are fused together in the 'UPN' construct), marking all male-specific neurons. These reporter genes measure a wide variety of phenotypic features of a neuron, including

Development (2021) 148, dev199687. doi:10.1242/dev.199687

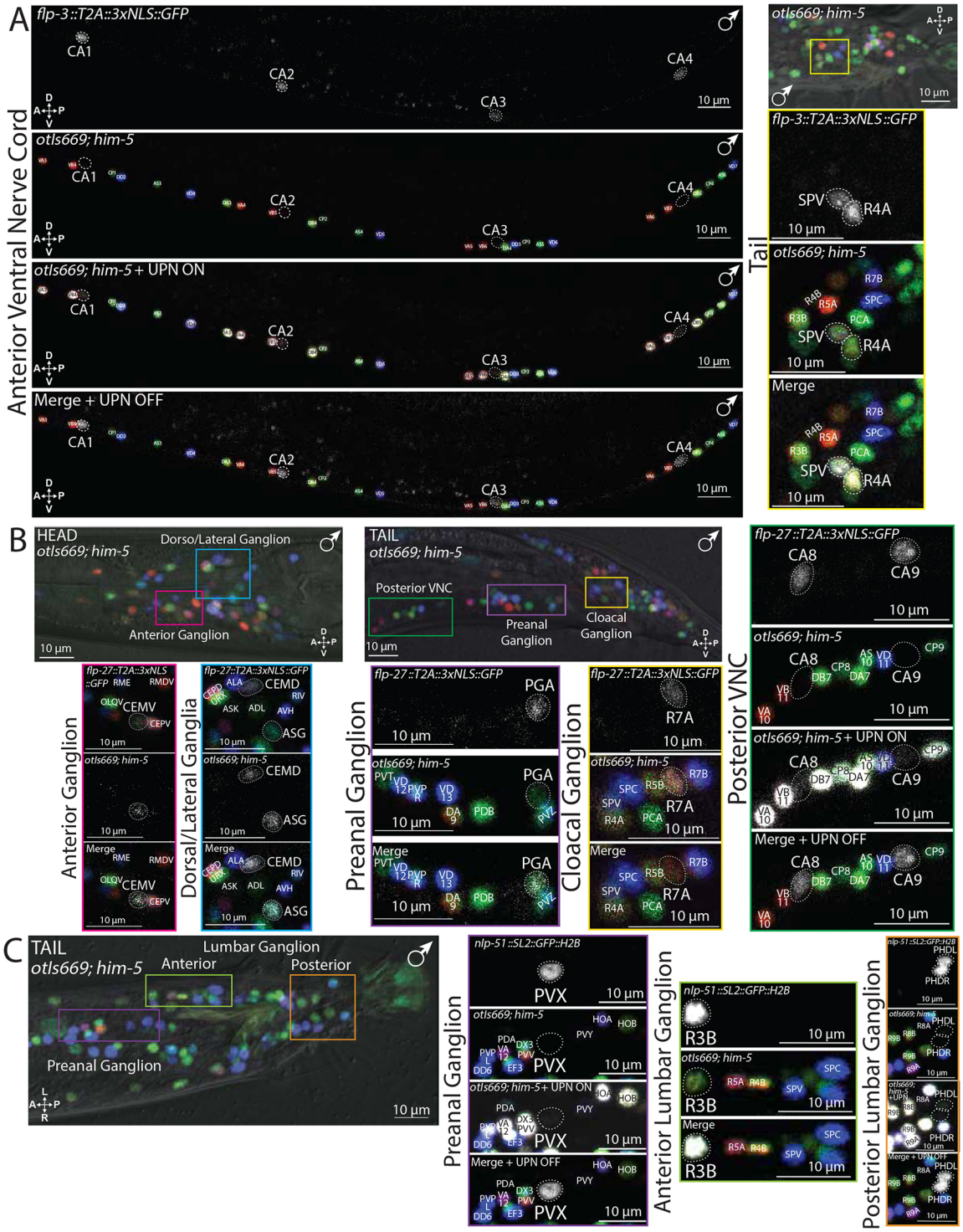

Fig. 4. Using NeuroPAL for identification of *gfp*-based expression patterns. (A) NeuroPAL (*otIs669; him-5*) is used to identify the GFP expression profile of a *gfp*-tagged neuropeptide gene, *flp-3(syb2634[T2A::3xNLS::GFP])*, in the male ventral nerve cord (VNC) and the tail. The anterior VNC is depicted on the left-hand side. On the right-hand side, an overview of the male tail is shown in the top image with inset images (outlined in yellow) below. (B) NeuroPAL is used to identify the GFP expression profile of a *gfp*-tagged neuropeptide gene, *flp-27(syb3213[T2A::3xNLS::GFP])*, in the male head, posterior VNC, preanal ganglion and lumbar ganglion. An overview of the head is shown with inset images that correspond to the anterior ganglion (outlined in magenta) and the dorso/lateral ganglia (highlighted in light blue). In the posterior VNC, it is expressed in the male-specific neurons CA8 and CA9, and in the male-specific neuron PGA in the preanal ganglion. In the lumbar ganglion, it is expressed in the male-specific ray neuron R7A, and it is variably dimly expressed (not pictured) in R6B. An overview picture of the male tail is shown with inset images that correspond to the preanal ganglion (outlined in purple), the posterior VNC (outlined in green) and the cloacal ganglia (outlined in yellow). (C) NeuroPAL is used to identify the GFP expression profile of a neuropeptide gene, *nlp-51(syb3936[SL2::GFP::H2B)*, in the male tail. An overview picture of the male tail is shown with inset images that correspond to the preanal ganglion (outlined in purple), the anterior lumbar ganglion (outlined in green), and the posterior lumbar ganglion (outlined in orange). *nlp-51* is also expressed in the sex-shared neurons RIP, AIM and PVN, as well as variably expressed in the male-specific neuron R4B (not pictured).

Development (2021) 148, dev199687. doi:10.1242/dev.199687

neurotransmitter synthesis and transport, neurotransmitter receptors, neuropeptides, sensory receptors from various families, and pan-neuronal features (Table S1) (Yemini et al., 2021). The markers therefore provide a panoramic view of the differentiated state of all individual neurons, and this state can be probed for proper execution in mutant backgrounds.

We illustrate the utility of NeuroPAL for such mutant analysis using three prominent patterning genes: a miRNA (*lin-4*) (Lee et al., 1993), a HOX cluster gene (*egl-5/AbdB*) (Chow and Emmons, 1994) and a proneural bHLH gene (*lin-32/Atonal*) (Zhao and Emmons, 1995). The functions of these genes have been reported for only select parts of the male-specific nervous system (Chalfie et al., 1981; Chow and Emmons, 1994; Zhao and Emmons, 1995). We sought to assess whether their reported defects can be recapitulated and better characterized with NeuroPAL. Furthermore, we anticipated identifying novel defects in these mutants in previously unexamined parts of the male-specific nervous system. Both of these expectations were fulfilled in all three cases examined, as described in the following sections.

NeuroPAL confirms predicted neuron losses and duplications in *lin-4* miRNA mutants and identifies additional neuronal defects

Animals lacking the *lin-4* miRNA display an iteration of cellular fates normally executed at the first larval stage (Chalfie et al., 1981; Lee et al., 1993), as inferred mainly from analysis of the ectodermal V and T ectoblasts in the male. Specifically, based on cellular cleavage patterns and neuron-like nuclear morphologies, L1 stage-specific T-cell neurons appear to be duplicated, whereas T-derived ray neurons that are normally generated at late larval stages do not appear to be generated (Chalfie et al., 1981) (redrawn in Fig. 5B). We extended these previous findings through our ability to visualize neuronal differentiation programs with greater detail using NeuroPAL. We confirmed that T-derived ray neurons are not generated in *lin-4* mutant animals whereas neurons displaying the color code of the T cell-derived PHC, PHD, PLN and PVW appear to be duplicated (Fig. 5C). Similarly, the V5 lineage-derived ray neurons R1A/B and R2A/B, normally generated at the L4 stage, failed to be generated in *lin-4* mutants (Fig. 5D).

Cleavage defects in other lineages that produce male-specific neurons (B, Y, U, F) had been noted in *lin-4* mutant males (Chalfie et al., 1981), but whether and to what extent neuronal fate specification is disrupted in these lineages remained unclear. We observed no cells with color codes representative of neurons derived from the B, Y and F-blast cells, which are normally born at late larval stages (Fig. 5C,E). This parallels the effect of *lin-4* on the late-born neurons in the T and V lineage and underscores that in *lin-4* mutants development is arrested in a juvenile state. The color patterns in the preanal ganglion, where U cell descendants are normally located, was too complex to interpret, and therefore we cannot infer the nature of defects in this lineage.

We also found that the fate of all late-born, male-specific neurons that are generated by the P neuroblast are lost in *lin-4* mutant animals. In the tail, male-specific neuronal cell fates derived from the P10 and P11 lineages (HOA, HOB, etc.) appeared to be lost. Lastly, in the ventral nerve cord, we observed a loss of color codes of the CA8-9 and CP8-9 neurons (Fig. 5F). These neurons are normally generated by a cell division event at the L3 stage, and this division is possibly absent in *lin-4* mutants. In contrast, P cell-derived ventral nerve cord motor neurons, which are generated in both sexes at early larval stages, differentiated normally in *lin-4* null mutants (Fig. 5F).

NeuroPAL identifies homeotic identity transformations in *egl-5* mutants

The B, Y, U and F ectoblasts, which divide exclusively in males, express the HOX cluster protein EGL-5/AbdB (Ferreira et al., 1999). In *egl-5* mutants, these ectoblasts fail to undergo proper divisions and generate no neurons (Chisholm, 1991). This conclusion was based on light-microscopy criteria, i.e. absence of characteristic dense neuronal nuclei. Using the neuronal cell fate markers present in the NeuroPAL transgene, we further corroborated this notion: none of the colored neurons that descend from B, Y, U and F (Fig. 1B) could be observed in *egl-5* mutants (Fig. 6).

Previous work has revealed an anterior-posterior patterning role of the HOX genes *mab-5* and *egl-5* in the ray lineage (Emmons, 2005). Ray neuron 2 is MAB-5 positive and EGL-5 negative, whereas ray neurons 3 to 6 are EGL-5 positive (Lints et al., 2004). It was suggested that in *egl-5* mutants, rays 3, 4 and 5 homeotically transform to the fate of ray 2 neurons. With the limited markers available at the time, this suggestion remained tentative (Lints et al., 2004). We verified this suggestion by confirming that color code changes in NeuroPAL are consistent with a ray 2 neuron identity transformation (Fig. 6B).

Using NeuroPAL, we discovered an additional homeotic identity transformation in the posterior-most, male-specific CA motor neurons. The CA8 and CA9 neurons adopted similar color codes to the more-anterior CA7 neuron (Fig. 6C). These transformations are conceptually similar to the homeotic transformations observed in the sex-shared, posterior-most DA and AS neurons in *egl-5* mutants where the most posterior class member also transforms its identity to that of the more anteriorly located neuron (Kratsios et al., 2017).

NeuroPAL confirms the proneural function of *lin-32*/*Ato* in ray lineages and reveals additional proneural function in other lineages

The single ortholog of the proneural Atonal gene in *C. elegans*, *lin-32*, was initially identified and characterized based on its proneural role in V5 and V6 ectoblast-derived ray neurons (Zhao and Emmons, 1995). Using NeuroPAL, we observed variable loss of neuronal fate specification in the ray lineage in *lin-32(tm1446)* mutants in the V5- and V6-derived ray neurons, as evidenced by missing color codes in these neurons, including the pan-neuronal color (Fig. 6E,F). The most-posterior ray neurons, generated by the T lineage (Fig. 1B), were unaffected in *lin-32* null mutants, as were all of the other T-derived neurons (Fig. 6E,F). Y-, U- and F-derived neurons, as well as P cell-derived, male-specific VNC motor neurons (see lineage diagram in Fig. 1B) were also unaffected in *lin-32* mutants (Fig. 6G,H). However, within the B lineage, we discovered a proneural role of *lin-32* mutants. Whereas the neurons generated by the posterior daughter of the B ectoblast cell (DVE and DVF, located in the dorsorectal ganglion) differentiated normally, the neuronal cell fates generated by the anterior daughter of B (mostly spicule neurons) could not be detected (Fig. 6E,G).

NeuroPAL reveals a coordinated differentiation wave that is concomitant with male tail retraction

We next used NeuroPAL as a tool to provide a panoramic view of timing of neuronal differentiation in the male tail. As illustrated in Fig. 1B, male-specific neurons are generated at multiple distinct developmental stages. Some male-specific neurons are generated in the embryo (CEM neurons), more are generated at the first larval stage (e.g. PVX of the P cell lineage), the L2 stage (e.g. PCB), the L3 stage (B and P cell descendants) and the L4 stage (mostly ray

Development (2021) 148, dev199687. doi:10.1242/dev.199687

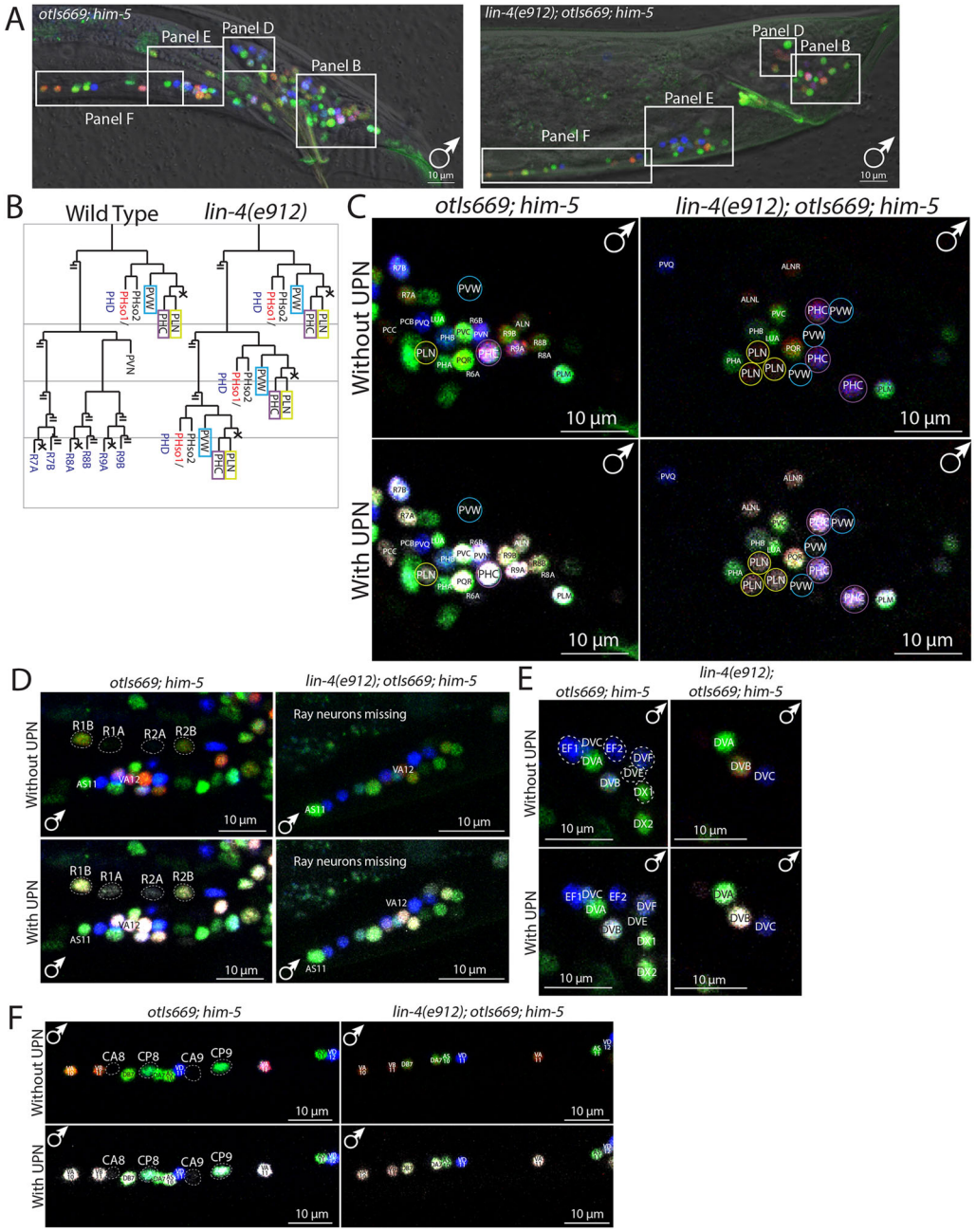

Fig. 5. NeuroPAL visualizes neuronal-patterning defects in miRNA *lin-4* mutants. (A) Micrographs of the posterior VNC and tails of wild-type and *lin-4* mutant males with boxes indicating from which regions each panel was derived. (B) Lineage diagrams depicting the wild-type T lineage on the left and the *lin-4* mutant T lineage exhibiting lineage reiterations in the L1-specific T lineage, as reported by Chalfie et al. (1981). Only those lineage branches containing neurons are depicted to the end, cells that die are represented with an X, and all other branches are cut off (depicted by double strike through). The names of sex-shared neurons are depicted in black, hermaphrodite-specific neurons in red and male-specific neurons in blue. (C) Lineage iterations in the L1-specific T lineage, first reported by Chalfie et al. (1981), are confirmed with NeuroPAL, as evidenced by the presence of additional neurons with the distinct NeuroPAL color barcodes of PLN, PHC and PVW in the tail of *lin-4(e912)* males. The left image depicts a wild-type male NeuroPAL tail with a single PLN neuron (yellow circle), a single PHC neuron (purple circle) and a single PVW neuron (blue circle). In contrast, the *lin-4(e912)* mutant male tail contains three PLN neurons (yellow circles), three PHC neurons (purple circles) and three PVW neurons (blue circles), all distinguished by their NeuroPAL coloring. Twenty animals were scored and all animals exhibited reiterations in the L1-specific T lineage. (D) Male-specific ray neurons (R1A, R1B, R2A, R2B) generated from the V5 lineage, and highlighted by dashed circles, are missing in *lin-4(e912)* mutants. Male-specific ray neurons were never observed in the 20 scored worms. Male-specific neurons generated from the B and F lineages in the dorsorectal ganglion (DRG), indicated by dashed circles in the image of NeuroPAL on its own, are missing in *lin-4(e912)* mutants. In contrast, sex-shared neurons (DVA, DVB and DVC) remain in *lin-4(e912)* mutants. Twenty animals were scored and neurons from the B and F lineages in the DRG were never observed. (E) Male-specific neurons generated from the B and F lineages in the DRG, indicated by dashed circles in the image of NeuroPAL on its own, are missing in *lin-4(e912)* mutants. In contrast, sex-shared neurons (DVA, DVB and DVC) remain in *lin-4(e912)* mutants. Twenty animals were scored and neurons from the B and F lineages in the DRG were never observed. (F) The color codes of the L3-specific CA8-9 and CP8-9 neurons in the male VNC are missing in *lin-4(e912)* mutants, whereas the L1-specific neurons VA, VB, VD are unaffected, as evidenced by the expression of their proper NeuroPAL colors. In the 20 animals that were scored, the color codes of the CA8 and CP8 neurons were never observed, but the color code of CA9 was observed in one animal, and the color code of CP9 was observed in five animals.

Development (2021) 148, dev199687. doi:10.1242/dev.199687

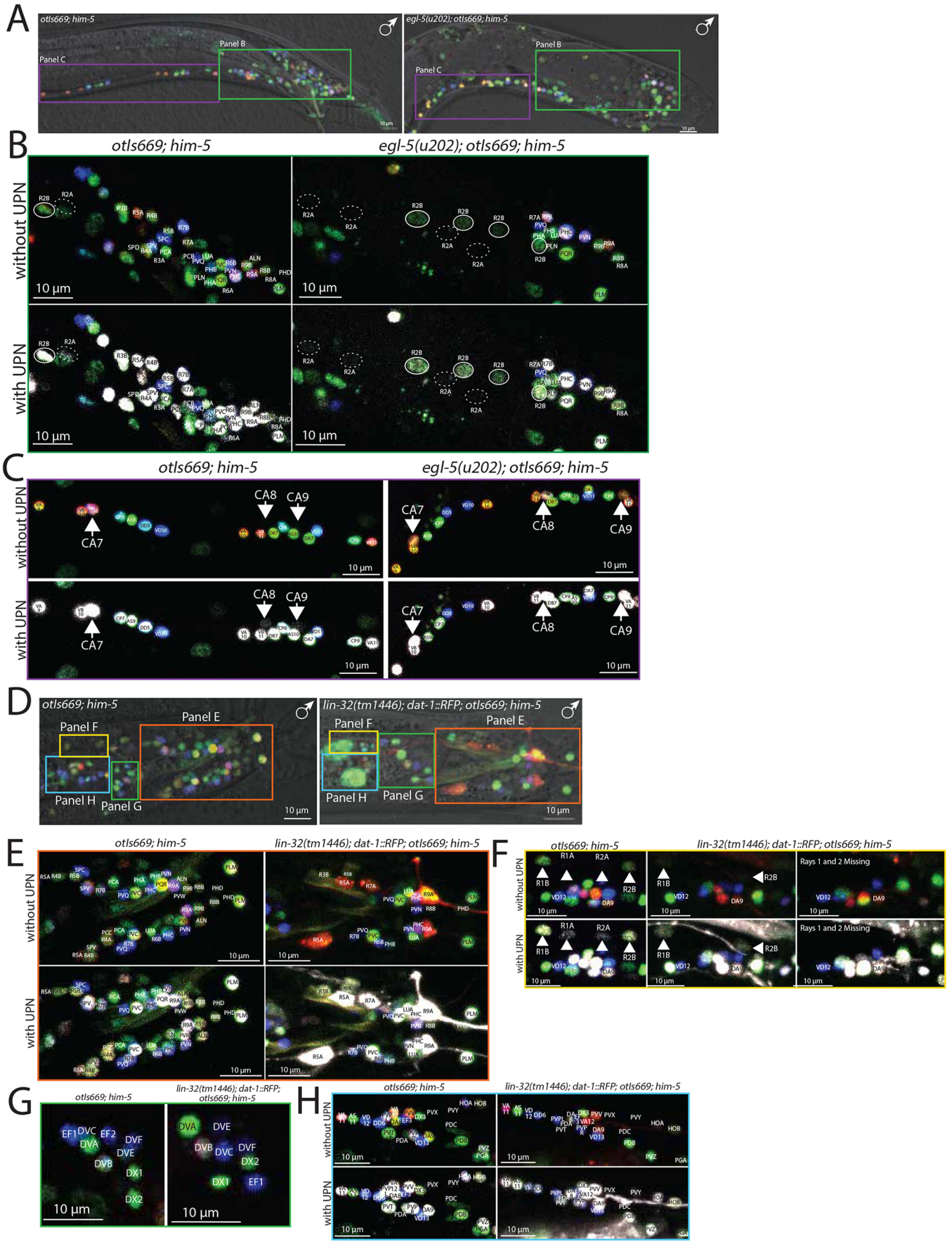

Fig. 6. See next page for legend.

Development (2021) 148, dev199687. doi:10.1242/dev.199687

Fig. 6. NeuroPAL visualizes patterning defects in transcription factor mutants. (A-C) Patterning defects in the VNC of *egl-5* Hox mutant males are visualized using NeuroPAL (*otIs669; him-8*). (A) Micrographs of the posterior VNC and tails of wild-type and *egl-5* mutant males with boxes indicating regions from which each following panels are derived. The region of the tail from which panel B is derived is outlined in green and the region from which panel C is derived is outlined in purple. (B) Transformations of the ray neurons, R3, R4 and R5 to that of a R2 neuron fate was described by Lints et al., 2004. Here, the A-type neurons (R3A, R4A, R5A) are denoted by dashed circles and the B-type neurons (R3B, R4B, R5B) are denoted by solid-line circles. In e*gl-5(u202)* mutant males, there is a loss of the NeuroPAL colors of the A- and B-type R3, R4 and R5 neurons and a gain of three R2A and three R2B neurons. The transformation of R3, R4 and R5 was observed in all 14 animals that were scored. (C) The arrows denote CA7, CA8 and CA9 neurons in NeuroPAL and *egl-5(u202)*; NeuroPAL males. CA8 and CA9, normally marked only by the pan-neuronal marker in NeuroPAL, take on a distinct color, similar to CA7, in *egl-5(u202)* males. The transformation of CA8 and CA9 neurons was found in all 14 animals that were scored. (D-H) Patterning defects in *lin-32(tm1446)* bHLH mutant animals, visualized with *otIs669.* The *lin-32* mutant strain also carries a cytoplasmic *dat-1::RFP* reporter in the background, which marks dopamine neurons and corroborates the defects observed with NeuroPAL. The cytoplasmic *dat-1::RFP* reporter expression is easily distinguished from the nuclear expression of NeuroPAL. (D) Micrographs of the posterior VNC and tails of wild-type and *lin-32* mutant males with boxes indicating the regions from which each following panel are derived. The region of the tail from which E is derived is outlined in orange, F is outlined in yellow, G is outlined in green and H is outlined in blue. (E) A representative image of a *lin-32(tm1446)* male depicts variable loss of male ray neurons in the tail. Although posterior ray neurons are observed in most *lin-32* mutant male tails, other ray neurons are variably identifiable by their NeuroPAL color. Out of the 15 *lin-32(tm1446)* males that were scored, all showed some defects in ray neurons. Within the same animal the presence of ray neurons often differed between the left and right side, as pictured. (F) Variable loss of ray neurons R1B and R2B was observed in *lin-32(tm1446)* males. Two example images from *lin-32* mutant males are shown next to a wild-type NeuroPAL image of the region of interest. In the middle *lin-32(tm1446)* image, R1B and R2B are present and properly colored, whereas in the bottom *lin-32(tm1446)* image both R1B and R2B are missing, thus demonstrating their variability in *lin-32* mutant males. Out of the 15 animals scored, nine had neither R1B nor R2B, three had one R2B, and three had both R1B and R2B. (G) All neurons in the DRG are unaffected in *lin-32(tm1446)* males as evidenced by the preservation of all NeuroPAL colors. Out of the 15 animals scored none of the *lin-32* mutant males showed defects in the DRG. (H) All neurons in the preanal ganglion (PAG) are unaffected in *lin-32(tm1446)* males as evidenced by the preservation of all NeuroPAL colors. Out of the 15 animals scored none of the *lin-32* mutant males showed defects in the PAG. In B-H, the upper images are NeuroPAL without the pan-neuronal marker ('UPN'-based), whereas the lower images include this marker in white.

sensory neurons) (Sulston et al., 1980). Strikingly, we found that, despite their distinct generation time, the expression of the more than 40 terminal differentiation markers (located on the NeuroPAL transgene) are tightly coordinated over a relatively small window during the mid-to-late L4 stage (Fig. 7, Fig. S3). At early L4, color codes are not yet established (Fig. 7), nor are they at earlier larval stages (Fig. S3). The mid-to-late L4 stage is concomitant with the beginning of male tail retraction, a sexually dimorphic process that results in the generation of male-specific mating organs (Emmons, 2005; Nguyen et al., 1999; Sulston et al., 1980). The extent of this coordination is striking, not only because of the substantial number of cell types over which we observed this coordination, but also because of the breadth of the distinct molecular features that are covered by these molecular markers. Among the components of this marker set are the *cis*-regulatory elements from four distinct pan-neuronal genes (*unc-11*, *rgef-1*, *ehs-1*, *ric-19*). Like the neuron-class-specific marker genes, all these elements only begin to drive reporter gene expression during the mid-to-late L4 stage, concomitant with male tail retraction.

None of the markers for which we observed a coordinated, delayed onset during the L4 stage in sex-specific neurons displayed a delay in sex-shared and embryonically born neurons. That is, all NeuroPAL markers turn on after sex-shared neuron birth and remain stable throughout all larval stages (Fig. S3). The best illustration of the specificity of the coordinated expression wave in male-specific neurons are sex-shared neurons that are born in both sexes at similar stages of larval development. We consistently found that, in all cases, the NeuroPAL color code turned on shortly after the generation of these neurons (i.e. after their terminal cell division) (Fig. S3). For example, the sex-shared PDB and VD13 neurons, both close lineal relatives to the male-specific PVX neuron, were born at about the same time as the male-specific PVX (Fig. 1B). Whereas PVX generated its color code only at the L4 stage, PDB and VD13 generated their color code much earlier, at the late L1 stage that occurs soon after their birth (Fig. S3). Similarly, the L2-generated, male-specific PCB neuron class turned on its color code at the mid-to-late L4 stage, whereas the L2-generated, but sex-shared RMF neuron class and the L2-generated neurons of the postdeirid lineage generated their color codes shortly after their birth (Fig. 7).

In order to not be entirely reliant on the NeuroPAL transgene in assessing the timing of neuronal differentiation, we examined whether the delayed, coordinated onset of molecular differentiation features can be observed with other reporters as well. To this end, we utilized fosmid-based reporters for three genes, the pan-neuronally expressed *rab-3* gene (*otIs498*), the synaptic organizer *oig-1* (*otIs450*) and the vesicular transporter *unc-47* (*otIs564*), as well as three reporter alleles in which endogenous genes were tagged with *gfp* through CRISPR/Cas9 genome engineering, namely the neuropeptide-encoding genes *flp-27* and *nlp-51* and the vesicular glutamate transporter *eat-4*. Whereas *rab-3* was expressed in all male-specific neurons, *oig-1*, *unc-47*, *flp-27*, *nlp-51* and *eat-4* were expressed in a select subset of male-specific neurons, generated before the L4 stage. We found that all of these genes only turned on expression at the L4 stage (Fig. 8). The delay in onset of expression compared with generation of the neuron is too long to be explained by fluorescent protein maturation alone.

Lastly, we investigated whether the delayed differentiation onset of male-specific neurons depends on the sexual identity of the animal. To this end, we prevented cell death of the CEM neurons in hermaphrodites, using a canonical *ced-3* mutant allele (Ellis and Horvitz, 1986), and assessed the onset of expression of the CEM differentiation marker *pkd-2::gfp* in these animals. If the proper timing of *pkd-2* induction would require the animal to have a male identity (for example, if male-specific cells are required to induce *pkd-2* expression), *pkd-2::gfp* expression should either not be induced or be initiated at an improper stage (e.g. right after the birth of the neurons). However, we found that *pkd-2::gfp* expression is still timed to the L4 stage of *ced-3* mutant hermaphrodites (Fig. S4). Hence, male-specific cues are not required to time CEM differentiation properly.

We conclude that earlier born male-specific neurons delay their differentiation until the fourth larval stage and then differentiate in a coordinated manner, concomitantly with the differentiation of sexual organs.

DISCUSSION

The nervous system of the *C. elegans* male contains almost 30% more neurons than the hermaphrodite. The male-specific nervous

Development (2021) 148, dev199687. doi:10.1242/dev.199687

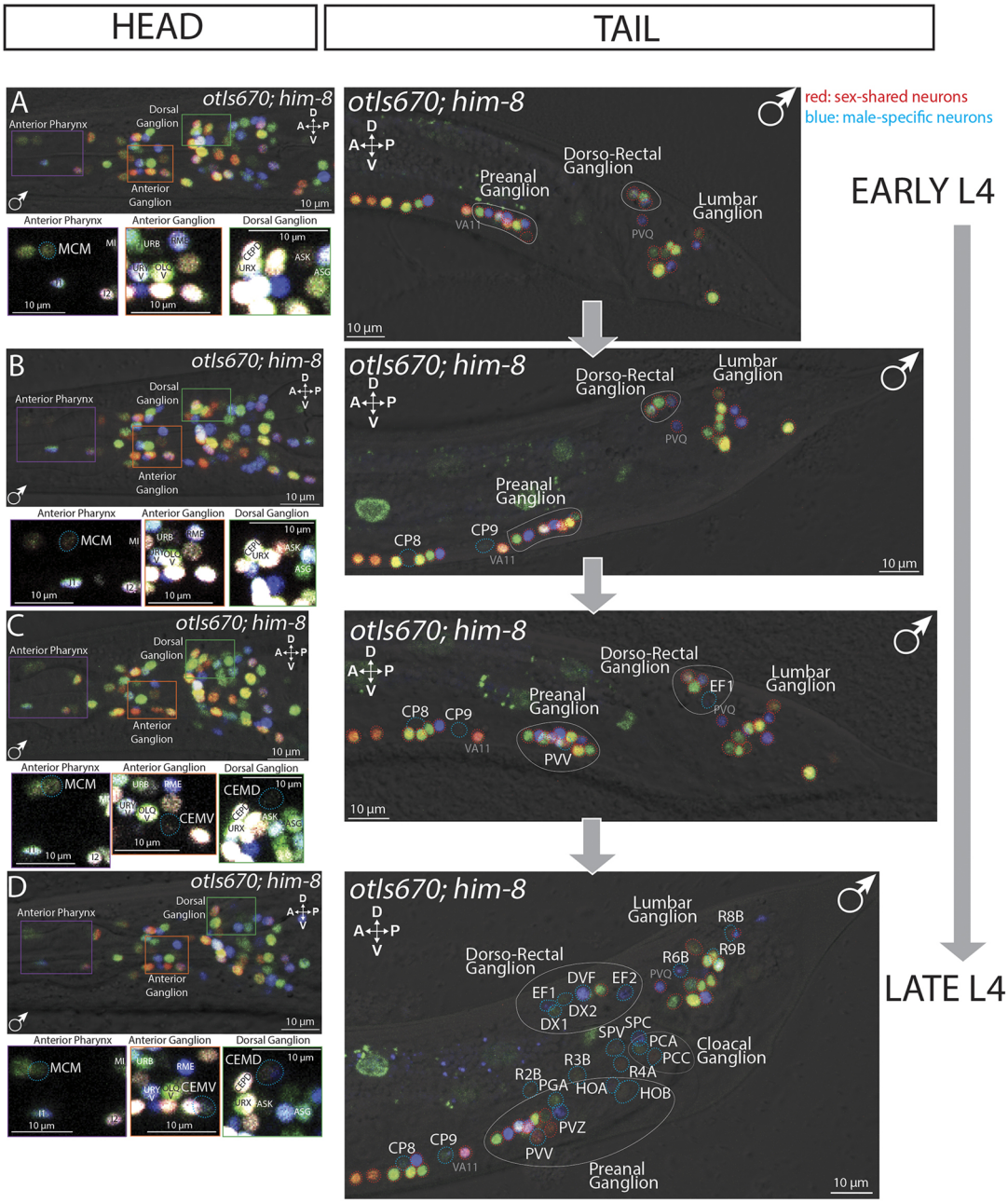

Fig. 7. Just-in-time differentiation revealed by temporal appearance of NeuroPAL color codes. Male-specific NeuroPAL (*otIs670; him-8*) neuronal color code emergence is coordinated with male maturation and retraction of the male tail, which occurs 4 h before the L4-to-adult molt. The leftmost panels depict representative images of NeuroPAL expression in the heads of L4 males. Inset images show NeuroPAL and the pan-neuronal marker in the following ganglia: the anterior pharynx (outlined in purple), anterior ganglion (outlined in orange) and dorsal ganglion (outlined in green). The right-hand panels show male tail NeuroPAL expression and differential interference contrast (DIC) micrographs from the early to late L4 larval stage. Sex-shared neurons are indicated with red dashed circles. Male-specific neurons are indicated with blue dashed circles and labeled with their neuron names. Some sex-shared neurons (e.g. VA11 in the preanal ganglion and PVQ in the lumbar ganglion) are labeled to aid the reader in orienting themselves within the worm's ganglia. Each worm's head and tail were imaged in order to use the timing of the male tail retraction to precisely define their age during the L4 larval stage; see Materials and Methods for further details on staging. (A) A representative image of an early L4 male NeuroPAL (*otIs670; him-8)* head with inset images from the indicated regions below, and an age-matched male tail on the right. At this stage, only sex-shared neurons and the male-specific neuron MCM express their NeuroPAL colors. (B) A representative image of a mid-early stage L4 male NeuroPAL (*otIs670; him-8)* head. Inset images from the indicated head regions are shown below and an age-matched tail on the right is shown that has just begun to retract. At this stage, the male-specific neurons CP8 and CP9 are beginning to express their adult NeuroPAL color codes as indicated by the blue dashed circles. (C) A representative image of a mid-late stage L4 male NeuroPAL (*otIs670; him-8*) head. Inset images from the indicated head regions are shown below and an age-matched tail on the right is shown in which the tail tip hypodermal cells, hyp9 and hyp10, have retracted. At this stage in the head, the male-specific neurons CEMV and CEMD are beginning to express the pan-neuronal marker as indicated by the blue dashed circles. At this stage in the tail, the male-specific neurons PVV and EF1 are beginning to express their adult NeuroPAL color codes as indicated by the blue dashed circles. (D) Representative image of a late stage L4 male NeuroPAL (*otIs670; him-8*) head. Inset images from the indicated head regions are shown below along with an age-matched tail. At this stage, many of the male-specific neurons are taking on their adult NeuroPAL color in the tail as indicated by the blue dashed circles.

Development (2021) 148, dev199687. doi:10.1242/dev.199687

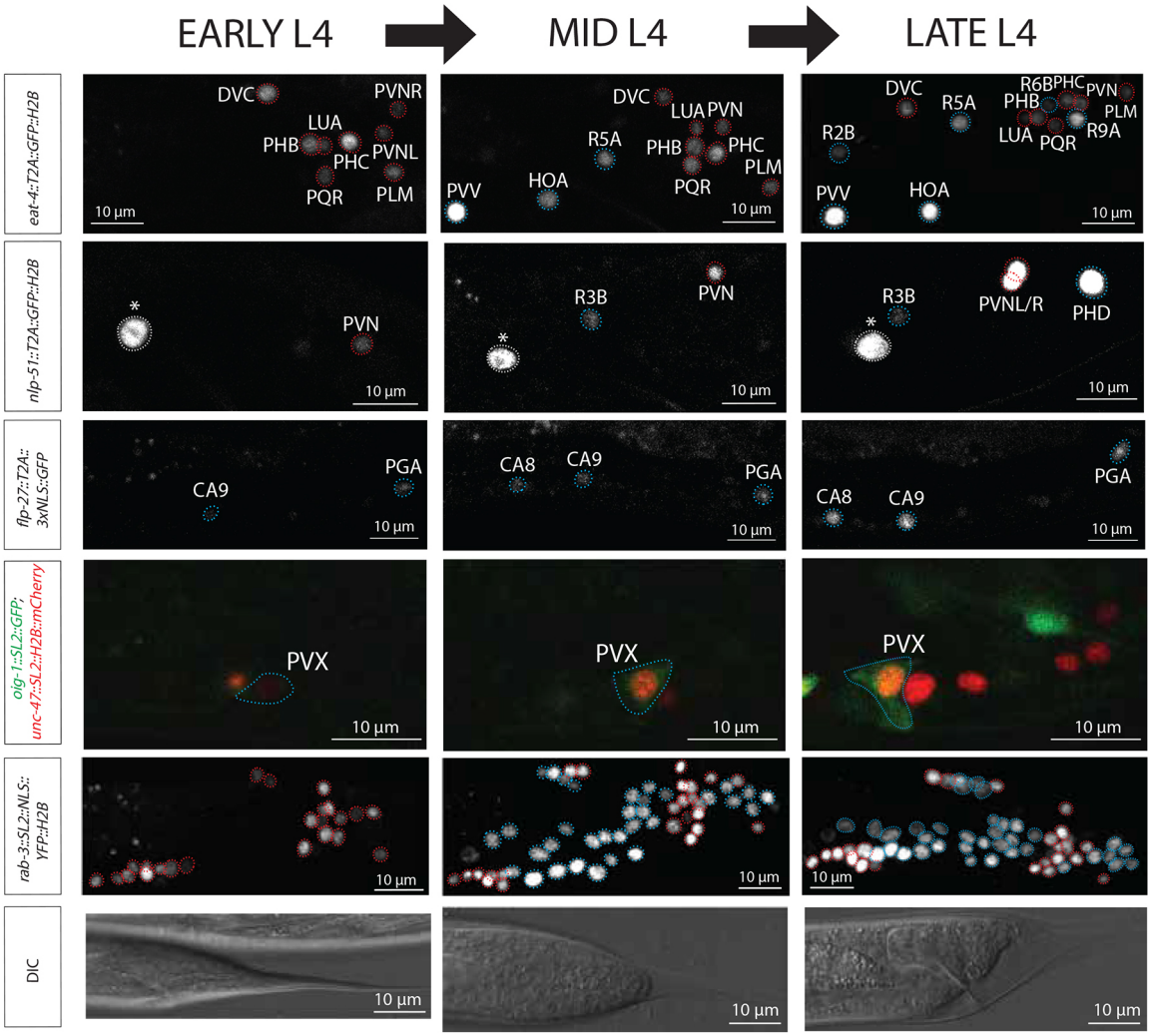

Fig. 8. Just-in-time differentiation confirmed with additional reporter genes. Expression of three fosmid-based reporters, the pan-neuronally expressed *rab-3* gene (*otIs498)*, the synaptic organizer *oig-1 (otIs450)* and the vesicular transporter *unc-47 (otIs564)*, as well as three reporter alleles in which endogenous genes were tagged with *gfp* through CRISPR/Cas9 genome engineering – the neuropeptide-encoding genes *flp-27(syb3213[T2A::3xNLS::GFP])* and *nlp-51(syb3936[SL2::GFP::H2B])* and the vesicular glutamate transporter *eat-4(syb4257[T2A::GFP::H2B])* – are shown. Onset and/or strong upregulation was consistently observed during the mid-to-late L4 stage of development (see Materials and Methods for staging). Male-specific neurons are indicated with blue dashed circles and, when possible, labeled with their neuron name. Sex-shared neurons are indicated with red dashed circles and, when possible, labeled with their neuron name. Non-neuronal cells are indicated with white dashed circles and an asterisk. In all cases except for *oig-1* and *unc-47*, NeuroPAL was used in the background to identify neurons.

system is structurally complex and controls the many intricate steps of male-mating behavior (Garcia et al., 2001; Liu and Sternberg, 1995; Barr et al., 2018; Portman, 2017). From a developmental perspective, it is fascinating to ask how complex interconnected circuitry is established during postembryonic development and integrated with an already existing, sex-shared nervous system. To address the many questions relating to the development and function of the male-specific nervous system, it is important to be able to characterize gene expression patterns and gene function, and to visualize male neuronal activity patterns. The tool that we present here, NeuroPAL, presents a major stepping stone to achieve these goals. NeuroPAL enables rigorous analysis of gene expression patterns and gene function in the male-specific nervous system. Moreover, the ability to combine NeuroPAL with GCaMP-based neuronal activity recordings – as recently shown in the hermaphrodite nervous system (Yemini et al., 2021) – will pave the way to decipher neuronal activity patterns reliably in the male nervous system.

Owing to its ability to visualize the expression of more than 40 distinct genes that reveal the live differentiated state of neurons throughout the entire nervous system of both sexes, we have been able to use NeuroPAL to gain insights into the development of the male-specific nervous system. We corroborated and extended the findings of an unusual non-stereotypic variability in the generation of a specific set of neurons, the EF and DX neurons. We further refined and also revealed the patterning roles of three gene regulatory factors: a Hox cluster gene, a miRNA and a bHLH transcription factor. Perhaps most interestingly, we used NeuroPAL to reveal that, despite their diverse birth dates, male-specific neurons coordinate the acquisition of terminal identity features to within a specific window of time, the mid-to-late fourth larval stage. At this time, other non-neuronal mating structures – including fans, rays and spicules – are generated (Emmons, 2005; Nguyen et al., 1999; Sulston et al., 1980). We term this coordinated differentiation ‘just-in-time’ differentiation, to illustrate that neurons only acquire their functional properties once all the ‘effector systems’ of the

Development (2021) 148, dev199687. doi:10.1242/dev.199687

male-specific nervous system (i.e. all the end organs innervated by the male-specific neurons) come into existence, and thus only once the mating process becomes physically possible as a result of the generation of such mating organs. It is important to emphasize the two reasons why just-in-time differentiation cannot merely be a reflection of a delay in maturation of the fluorophores with which we measure differentiation programs. First, fluorescent signals are visible in sex-shared neurons immediately after their generation at early larval stages, whereas male-specific neurons that are born concurrently show a delay of up to several larval stages (>24 h later); in contrast, fluorophore maturation times are known to operate on a much faster scale, with most maturing within <1 h (Balleza et al., 2018; Cranfill et al., 2016). Second, the birth dates of different male-specific neurons are distinct, yet the onset of fluorophore expression is coordinated to occur at the same time.

The 'just-in-time' terminology is adapted from 'just-in-time' specific transcriptional programs in metabolic pathways (Zaslaver et al., 2004). Genes that code for specific proteins in the metabolic production machinery display temporal dynamics which ensure that, when a metabolic production pipeline is being ramped up under specific conditions, proteins are generated only when needed in the production pipeline. This allows the machinery to reach a production goal with minimal total enzyme production (Zaslaver et al., 2004).

Coordinated, just-in-time differentiation programs are apparent throughout all male-specific neurons. For one of them, the CEM neurons, the delayed onset of differentiation had been previously noted before. The CEM neurons are born in the embryo (and die in hermaphrodites) but were reported to initiate expression of several molecular features, including the putative sensory receptor *pkd-2* and its cholinergic-neurotransmitter phenotype, only by the L4 stage (Lawson et al., 2019; Pereira et al., 2015; Wang et al., 2010). CEM neurons only synapse onto sex-shared neurons that were generated and already differentiated in the embryo (Cook et al., 2019), thus the just-in-time differentiation of CEMs at the L4 stage cannot simply relate to the appearance of sex-specific effector cells at the L4 stage. The reason that CEM differentiation is delayed until the L4 stage likely lies in their function: CEM neurons sample mating cues (Narayan et al., 2016; Srinivasan et al., 2008) and hence are not required to operate until the male is sexually mature.

Just-in-time differentiation is not unique to male-specific neurons. Hermaphrodite-specific neurons, of which there are only two classes, the HSN and VC neuron classes, had already been reported to acquire their fully differentiated state only at the L4 stage. In the HSN neurons, which are embryonically born, this is best evidenced by the acquisition of its serotonergic neurotransmitter identity, which they acquire at the late L4 stage (Desai et al., 1988). In the VC neurons, which are generated by the late first-larval stage, cholinergic marker gene expression only becomes induced at the L4 stage as well (Pereira et al., 2015). The logic of the just-in-time differentiation of the HSN and VC neurons is evident: they innervate vulval musculature that only becomes generated and properly placed during late-larval development (Sulston and Horvitz, 1977).

How is this coordinated, just-in-time differentiation wave genetically specified? For the proper timing of differentiation of the male-specific CEM and hermaphrodite-specific HSN neurons, the heterochronic pathway has been implicated (Lawson et al., 2019; Olsson-Carter and Slack, 2010). This pathway is composed of a series of sequentially activated gene-regulatory factors, including transcription factors, regulatory RNAs and translational regulators (Rougvie and Moss, 2013). However, the effects of this pathway on CEM and HSN timing was shown to be only partial (Lawson et al., 2019; Olsson-Carter and Slack, 2010), suggesting the involvement of other regulatory factors. For example, it can be envisioned that target-derived signals from synaptic partners help to coordinate the timing of just-in-time differentiation. Perhaps sex-specific neurons are under a 'differentiation arrest' that actively inhibits the execution of terminal differentiation. This notion is again inferred from the CEM and HSN neuron cases, the key identity specifier of which, the terminal selector UNC-86 (Lloret-Fernandez et al., 2018; Shaham and Bargmann, 2002), is already present in the CEM and HSN neurons since their birth (Finney and Ruvkun, 1990). Although UNC-86 is required for the expression of HSN and CEM differentiation markers that become induced at the L4 stage (Lloret-Fernandez et al., 2018; Shaham and Bargmann, 2002), it is apparently unable to induce these features until the time is right. Correctly timed induction might thus be achieved by an inhibitory mechanism that prevents UNC-86 function or, alternatively, by the absence of an essential UNC-86 co-factor, expression of which is temporally controlled.

An intrinsic feature of terminal differentiation programs of many, and perhaps all, *C. elegans* neurons may explain why terminal differentiation of sex-specific neurons appears to be an all-or-nothing event. In many, and perhaps all, *C. elegans* neurons, gene expression programs within a neuron are highly coordinated by the activity of terminal-selector transcription factors that become active right after the birth of a neuron in order to initiate terminal differentiation (Hobert, 2016). Triggering the entire differentiation program of a neuron prematurely, i.e. before needed, and thus not coordinated with the differentiation of other neurons, may send uninformative or even conflicting signals to the sex-shared nervous system. Just-in-time differentiation, coordinated over multiple cell and tissue types, ensures that individual components of a nervous system only go online once every individual component is set in place.

MATERIALS AND METHODS

Strains

The following mutant alleles were used in this study: *lin-4(e912)*, *egl-5(u202)*, *ced-3(n717)* and *lin-32(tm1446)*. The following reporter strains were used: NeuroPAL strains *otIs669; him-5* and *otIs670; him-8* (Yemini et al., 2021). The following fosmid-based reporters were used: *otIs450[oig-1(fosmid)::SL2::GFP]*, *otIs564[unc-47(fosmid)::SL2::mCherry::H2B]* and *otIs498[rab-3(fosmid)::SL2::NLS::YFP::H2B]*. The following CRISPR/Cas9-generated reporter strains were generated by SunyBiotech through insertion of a reporter cassette at the 3′ end of the respective gene: *flp-3(syb2634[T2A::3xNLS::GFP])*, *flp-27(syb3213[T2A::3xNLS::GFP])*, *nlp-51(syb3936[SL2::GFP::H2B])* and *eat-4(syb4257[SL2::GFP::H2B])*. The following promoter-based reporter was used: *myIs4[Ppkd-2::GFP+Punc-122::GFP] him-5(e1490)V* (Bae et al., 2006).

Analysis of NeuroPAL color codes of *egl-5*, *lin-32* and *lin-4* mutants was performed using a *him-5* mutation in the background. To rule out the contribution of the *him-5* mutation to color code changes in mutants, we compared the NeuroPAL color codes in naturally induced males versus *him-5* males. We examined all neurons, both sex shared and male specific, and found no differences in color code.

Microscopy

Worms were anaesthetized using 20 mM sodium azide and were mounted on 5% agarose pads. Images were acquired on a Zeiss LSM880 confocal microscope, equipped with seven laser lines (405, 458, 488, 514, 561, 594 and 633 nm) and processed using ImageJ software. Gamma was adjusted for maximal color distinction for all images. All reporter and mutant strains were imaged at 40× magnification.

Staging of worms

To obtain worms staged throughout larval development, adult hermaphrodites were allowed to lay eggs for 1 h. After 1 h, the hermaphrodites were removed from the plates. The plates were then stored

at 20°C until the time points corresponding to each larval stage when they were imaged. To capture the early, mid (when the tail hypodermal cells retract), and late L4 stages, worms were imaged at ∼44 h, ∼52 h and ∼55 h, respectively, after egg laying and storage at 20°C. As there is some variability even within carefully staged worms, each L4 stage was confirmed by the male tail morphology.

Variability in cell position

To generate the statistical atlases of male neuron positions, their variability, and colors, we used our previously published strategy (Yemini et al., 2021). Briefly, we initialized the atlas to be the point cloud of one of the worms, then iteratively aligned each animal's neuron position point cloud to the current atlas, until all animals were aligned. These point clouds, which represent neuron positions and colors, were extracted from images of 12 male heads and 13 male tails that were manually annotated. Males were age-matched to those used in our previously published hermaphrodite atlas (Yemini et al., 2021). For each neuron, the atlas includes a mean position, a mean color and a covariance matrix representing the variability for the neuron's position and color across the population of worms. We computed the positions of the male and hermaphrodite neurons using the determinant of the neuron's positional covariance matrix as an estimate of their aligned spatial occupancy volume (Table S2). We used these volumes to compute differences in neuron position variability between hermaphrodites and males. To account for color variability resulting from any changes in the imaging hardware (e.g. aging equipment, such as excitation lasers), we affine-transformed the male atlas colors to those of the hermaphrodite using the sex-shared neurons. Color alignment and histogram matching have been previously shown to be a crucial step for downstream analysis in such computations as atlas creation and neural segmentation (Nejatbakhsh et al., 2020; Varol et al., 2020).

Acknowledgements

We thank Rene Garcia for help in distinguishing DVE and DVF, Maureen Barr for *pkd-2::gfp*, Laura Pereira for help in generating the male NeuroPAL map, and members of the Hobert lab for comments on the manuscript.

Competing interests

The authors declare no competing or financial interests.

Author contributions

Conceptualization: T.T., E.Y., O.H.; Methodology: T.T., E.Y.; Software: A.N.; Formal analysis: T.T., A.N.; Investigation: T.T., E.Y., C.W., R.W., N.M.; Data curation: T.T., E.Y.; Writing - original draft: O.H.; Writing - review & editing: T.T., E.Y., C.W., R.W.F.; Visualization: T.T., E.Y., A.N., C.W., R.W.F.; Supervision: E.Y., E.V., L.P., O.H.; Project administration: L.P., O.H.; Funding acquisition: L.P., O.H.

Funding

This work was funded by the National Institute of Neurological Disorders and Stroke (R37NS039996), the National Institute of Biomedical Imaging and Bioengineering (R01 EB22913) and the Howard Hughes Medical Institute. Deposited in PMC for release after 12 months.

Data availability

The imaging datasets for Figs 3B-H, 4, and S2, and Table S2 have been deposited in Zenodo (https://zenodo.org/record/5348578#.YS9tR45KhPZ and https://zenodo.org/record/5348591#.YS9tVY5KhPZ).

Peer review history

The peer review history is available online at https://journals.biologists.com/dev/article-lookup/doi/10.1242/dev.199687

References

Bae, Y.-K., Qin, H., Knobel, K. M., Hu, J., Rosenbaum, J. L. and Barr, M. M. (2006). General and cell-type specific mechanisms target TRPP2/PKD-2 to cilia. *Development* **133**, 3859-3870. doi:10.1242/dev.02555

Balleza, E., Kim, J. M. and Cluzel, P. (2018). Systematic characterization of maturation time of fluorescent proteins in living cells. *Nat. Methods* **15**, 47-51. doi:10.1038/nmeth.4509

Barr, M. M., García, L. R. and Portman, D. S. (2018). Sexual dimorphism and sex differences in caenorhabditis elegans neuronal development and behavior. *Genetics* **208**, 909-935. doi:10.1534/genetics.117.300294

Cao, J., Packer, J. S., Ramani, V., Cusanovich, D. A., Huynh, C., Daza, R., Qiu, X., Lee, C., Furlan, S. N., Steemers, F. J. et al. (2017). Comprehensive single-cell transcriptional profiling of a multicellular organism. *Science* **357**, 661-667. doi:10.1126/science.aam8940

Chalfie, M., Horvitz, H. R. and Sulston, J. E. (1981). Mutations that lead to reiterations in the cell lineages of C. elegans. *Cell* **24**, 59-69. doi:10.1016/0092-8674(81)90501-8

Chisholm, A. (1991). Control of cell fate in the tail region of C. elegans by the gene egl-5. *Development* **111**, 921-932. doi:10.1242/dev.111.4.921

Chow, K. L. and Emmons, S. W. (1994). HOM-C/Hox genes and four interacting loci determine the morphogenetic properties of single cells in the nematode male tail. *Development* **120**, 2579-2592. doi:10.1242/dev.120.9.2579

Cook, S. J., Jarrell, T. A., Brittin, C. A., Wang, Y., Bloniarz, A. E., Yakovlev, M. A., Nguyen, K. C. Q., Tang, L. T.-H., Bayer, E. A., Duerr, J. S. et al. (2019). Whole-animal connectomes of both Caenorhabditis elegans sexes. *Nature* **571**, 63-71. doi:10.1038/s41586-019-1352-7

Cranfill, P. J., Sell, B. R., Baird, M. A., Allen, J. R., Lavagnino, Z., de Gruiter, H. M., Kremers, G.-J., Davidson, M. W., Ustione, A. and Piston, D. W. (2016). Quantitative assessment of fluorescent proteins. *Nat. Methods* **13**, 557-562. doi:10.1038/nmeth.3891

Desai, C., Garriga, G., McIntire, S. L. and Horvitz, H. R. (1988). A genetic pathway for the development of the Caenorhabditis elegans HSN motor neurons. *Nature* **336**, 638-646. doi:10.1038/336638a0

Ellis, H. M. and Horvitz, H. R. (1986). Genetic control of programmed cell death in the nematode C. elegans. *Cell* **44**, 817-829. doi:10.1016/0092-8674(86)90004-8

Emmons, S. W. (2005). *Male Development. WormBook*, ed. The *C. elegans* Research Community, WormBook, doi:10.1895/wormbook.1.33.1

Emmons, S. W. (2014). The development of sexual dimorphism: studies of the Caenorhabditis elegans male. *Wiley Interdiscip. Rev. Dev. Biol.* **3**, 239-262. doi:10.1002/wdev.136

Emmons, S. W. (2018). Neural circuits of sexual behavior in Caenorhabditis elegans. *Annu. Rev. Neurosci.* **41**, 349-369. doi:10.1146/annurev-neuro-070815-014056

Ferreira, H. B., Zhang, Y., Zhao, C. and Emmons, S. W. (1999). Patterning of*Caenorhabditis elegans*posterior structures by the*Abdominal-B*homolog,*egl-5*. *Dev. Biol.* **207**, 215-228. doi:10.1006/dbio.1998.9124

Finney, M. and Ruvkun, G. (1990). The unc-86 gene product couples cell lineage and cell identity in C. elegans. *Cell* **63**, 895-905. doi:10.1016/0092-8674(90)90493-X

García, L. R. and Portman, D. S. (2016). Neural circuits for sexually dimorphic and sexually divergent behaviors in Caenorhabditis elegans. *Curr. Opin. Neurobiol.* **38**, 46-52. doi:10.1016/j.conb.2016.02.002

Garcia, L. R., Mehta, P. and Sternberg, P. W. (2001). Regulation of distinct muscle behaviors controls the C. elegans male's copulatory spicules during mating. *Cell* **107**, 777-788. doi:10.1016/S0092-8674(01)00600-6

Gendrel, M., Atlas, E. G. and Hobert, O. (2016). A cellular and regulatory map of the GABAergic nervous system of C. elegans. *eLife* **5**, e17686. doi:10.7554/eLife.17686

Hobert, O. (2016). Terminal selectors of neuronal identity. *Curr. Top. Dev. Biol.* **116**, 455-475. doi:10.1016/bs.ctdb.2015.12.007

Jarrell, T. A., Wang, Y., Bloniarz, A. E., Brittin, C. A., Xu, M., Thomson, J. N., Albertson, D. G., Hall, D. H. and Emmons, S. W. (2012). The connectome of a decision-making neural network. *Science* **337**, 437-444. doi:10.1126/science.1221762

Kalis, A. K., Kissiov, D. U., Kolenbrander, E. S., Palchick, Z., Raghavan, S., Tetreault, B. J., Williams, E., Loer, C. M. and Wolff, J. R. (2014). Patterning of sexually dimorphic neurogenesis in the caenorhabditis elegans ventral cord by Hox and TALE homeodomain transcription factors. *Dev. Dyn.* **243**, 159-171. doi:10.1002/dvdy.24064

Kratsios, P., Kerk, S. Y., Catela, C., Liang, J., Vidal, B., Bayer, E. A., Feng, W., De La Cruz, E. D., Croci, L., Consalez, G. G. et al. (2017). An intersectional gene regulatory strategy defines subclass diversity of C. elegans motor neurons. *eLife* **6**, e25751. doi:10.7554/eLife.25751

Lawson, H., Vuong, E., Miller, R. M., Kiontke, K., Fitch, D. H. A. and Portman, D. S. (2019). The Makorin lep-2 and the lncRNA lep-5 regulate lin-28 to schedule sexual maturation of the C. elegans nervous system. *eLife* **8**, e43660. doi:10.7554/eLife.43660

Lee, R. C., Feinbaum, R. L. and Ambros, V. (1993). The C. elegans heterochronic gene lin-4 encodes small RNAs with antisense complementarity to lin-14. *Cell* **75**, 843-854. doi:10.1016/0092-8674(93)90529-y

Lints, R. and Emmons, S. W. (1999). Patterning of dopaminergic neurotransmitter identity among Caenorhabditis elegans ray sensory neurons by a TGFbeta family signaling pathway and a Hox gene. *Development* **126**, 5819-5831. doi:10.1242/dev.126.24.5819

Lints, R., Jia, L., Kim, K., Li, C. and Emmons, S. W. (2004). Axial patterning of C. elegans male sensilla identities by selector genes. *Dev. Biol.* **269**, 137-151. doi:10.1016/j.ydbio.2004.01.021

Liu, K. S. and Sternberg, P. W. (1995). Sensory regulation of male mating behavior in Caenorhabditis elegans. *Neuron* **14**, 79-89. doi:10.1016/0896-6273(95)90242-2

Lloret-Fernández, C., Maicas, M., Mora-Martínez, C., Artacho, A., Jimeno-Martín, Á., Chirivella, L., Weinberg, P. and Flames, N. (2018). A transcription factor collective defines the HSN serotonergic neuron regulatory landscape. *eLife* **7**, e32785. doi:10.7554/eLife.32785

Molina-García, L., Lloret-Fernández, C., Cook, S. J., Kim, B., Bonnington, R. C., Sammut, M., O'Shea, J. M., Gilbert, S. P. R., Elliott, D. J., Hall, D. H. et al. (2020). Direct glia-to-neuron transdifferentiation gives rise to a pair of male-specific neurons that ensure nimble male mating. *eLife* **9**, e48361. doi:10.7554/eLife.48361

Narayan, A., Venkatachalam, V., Durak, O., Reilly, D. K., Bose, N., Schroeder, F. C., Samuel, A. D. T., Srinivasan, J. and Sternberg, P. W. (2016). Contrasting responses within a single neuron class enable sex-specific attraction in Caenorhabditis elegans. *Proc. Natl. Acad. Sci. USA* **113**, E1392-E1401. doi:10.1073/pnas.1600786113

Nejatbakhsh, A., Varol, E., Yemini, E., Hobert, O. and Paninski, L. (2020). *Probabilistic Joint Segmentation and Labeling of C. elegans Neurons*, Cham: Springer International Publishing.

Nguyen, C. Q., Hall, D. H., Yang, Y. and Fitch, D. H. A. (1999). Morphogenesis of the*Caenorhabditis elegans*male tail tip. *Dev. Biol.* **207**, 86-106. doi:10.1006/dbio.1998.9173

Olsson-Carter, K. and Slack, F. J. (2010). A developmental timing switch promotes axon outgrowth independent of known guidance receptors. *PLoS Genet.* **6**, e1001054. doi:10.1371/journal.pgen.1001054

Packer, J. S., Zhu, Q., Huynh, C., Sivaramakrishnan, P., Preston, E., Dueck, H., Stefanik, D., Tan, K., Trapnell, C., Kim, J. et al. (2019). A lineage-resolved molecular atlas of C. elegans embryogenesis at single-cell resolution. *Science* **365**, eaax1971. doi:10.1126/science.aax1971

Pereira, L., Kratsios, P., Serrano-Saiz, E., Sheftel, H., Mayo, A. E., Hall, D. H., White, J. G., LeBoeuf, B., Garcia, L. R., Alon, U. et al. (2015). A cellular and regulatory map of the cholinergic nervous system of C. elegans. *eLife* **4**, e12432. doi:10.7554/eLife.12432

Portman, D. S. (2017). Sexual modulation of sex-shared neurons and circuits in Caenorhabditis elegans. *J. Neurosci. Res.* **95**, 527-538. doi:10.1002/jnr.23912

Rougvie, A. E. and Moss, E. G. (2013). Developmental transitions in C. elegans larval stages. *Curr. Top. Dev. Biol.* **105**, 153-180. doi:10.1016/B978-0-12-396968-2.00006-3

Sammut, M., Cook, S. J., Nguyen, K. C. Q., Felton, T., Hall, D. H., Emmons, S. W., Poole, R. J. and Barrios, A. (2015). Glia-derived neurons are required for sex-specific learning in C. elegans. *Nature* **526**, 385-390. doi:10.1038/nature15700

Schafer, W. R. (2005). *Egg-Laying. WormBook*, ed. The *C. elegans* Research Community, WormBook, doi:10.1895/wormbook.1.38.1

Serrano-Saiz, E., Pereira, L., Gendrel, M., Aghayeva, U., Bhattacharya, A., Howell, K., Garcia, L. R. and Hobert, O. (2017). A neurotransmitter atlas of the Caenorhabditis elegans male nervous system reveals sexually dimorphic neurotransmitter usage. *Genetics* **206**, 1251-1269. doi:10.1534/genetics.117.202127

Shaham, S. and Bargmann, C. I. (2002). Control of neuronal subtype identity by the C. elegans ARID protein CFI-1. *Genes Dev.* **16**, 972-983. doi:10.1101/gad.976002

Srinivasan, J., Kaplan, F., Ajredini, R., Zachariah, C., Alborn, H. T., Teal, P. E. A., Malik, R. U., Edison, A. S., Sternberg, P. W. and Schroeder, F. C. (2008). A blend of small molecules regulates both mating and development in Caenorhabditis elegans. *Nature* **454**, 1115-1118. doi:10.1038/nature07168

Sulston, J. E. and Horvitz, H. R. (1977). Post-embryonic cell lineages of the nematode, Caenorhabditis elegans. *Dev. Biol.* **56**, 110-156. doi:10.1016/0012-1606(77)90158-0

Sulston, J. E., Albertson, D. G. and Thomson, J. N. (1980). The Caenorhabditis elegans male: postembryonic development of nongonadal structures. *Dev. Biol.* **78**, 542-576. doi:10.1016/0012-1606(80)90352-8

Taylor, S. R., Santpere, G., Weinreb, A., Barrett, A., Reilly, M. B., Xu, C., Varol, E., Oikonomou, P., Glenwinkel, L., McWhirter, R. et al. (2021). Molecular topography of an entire nervous system. *Cell* **184**, 4329-4347. doi:10.1016/j.cell.2021.06.023

Varol, E., Nejatbakhsh, A., Sun, R., Mena, G., Yemini, E., Hobert, O. and Paninski, L. (2020). *Statistical Atlas of C. elegans Neurons*, Cham: Springer International Publishing.

Wang, J., Schwartz, H. T. and Barr, M. M. (2010). Functional specialization of sensory cilia by an RFX transcription factor isoform. *Genetics* **186**, 1295-1307. doi:10.1534/genetics.110.122879

Yemini, E., Lin, A., Nejatbakhsh, A., Varol, E., Sun, R., Mena, G. E., Samuel, A. D. T., Paninski, L., Venkatachalam, V. and Hobert, O. (2021). NeuroPAL: A Multicolor Atlas for Whole-Brain Neuronal Identification in C. elegans. *Cell* **184**, 272-288.e11. doi:0.1016/j.cell.2020.12.012

Zaslaver, A., Mayo, A. E., Rosenberg, R., Bashkin, P., Sberro, H., Tsalyuk, M., Surette, M. G. and Alon, U. (2004). Just-in-time transcription program in metabolic pathways. *Nat. Genet.* **36**, 486-491. doi:10.1038/ng1348

Zhao, C. and Emmons, S. W. (1995). A transcription factor controlling development of peripheral sense organs in C. elegans. *Nature* **373**, 74-78. doi:10.1038/373074a0